

Position Tracking for Virtual Reality Using Commodity WiFi

Manikanta Kotaru, Sachin Katti
Stanford University

{mkotaru, skatti}@stanford.edu

Abstract

Today, experiencing virtual reality (VR) is a cumbersome experience which either requires dedicated infrastructure like infrared cameras to track the headset and hand-motion controllers (e.g. Oculus Rift, HTC Vive), or provides only 3-DoF (Degrees of Freedom) tracking which severely limits the user experience (e.g. Samsung Gear). To truly enable VR everywhere, we need position tracking to be available as a ubiquitous service. This paper presents WiCapture, a novel approach which leverages commodity WiFi infrastructure, which is ubiquitous today, for tracking purposes. We prototype WiCapture using off-the-shelf WiFi radios and show that it achieves an accuracy of 0.88 cm compared to sophisticated infrared based tracking systems like the Oculus, while providing much higher range, resistance to occlusion, ubiquity and ease of deployment.

1. Introduction

Immersive experiences like virtual reality (VR) require accurate tracking of the headset and other accessories like hand-motion controllers. Current commercial tracking systems like Oculus Rift [3] and HTC Vive [1] are outside-in where the tracking is performed using infrastructure external to the VR accessories. The external infrastructure is specialized and typically uses infrared (IR) cameras along with sensors on the headset to perform the tracking. These systems are very accurate but have the following limitations:

- They require installing specialized hardware and dedicated infrastructure wherever user wants to experience VR. So if a user wishes to use VR headsets anywhere in her home, one would need IR cameras everywhere.
- These systems are not occlusion resistant. For example, if the IR emitter is blocked by furniture, then the tracking stops working.
- These systems have limited range, typically around 2 m in front of the camera [6].

A competing technology to provide position tracking is inside-out position tracking found in systems like the Microsoft Hololens [2]. These systems use cameras (both

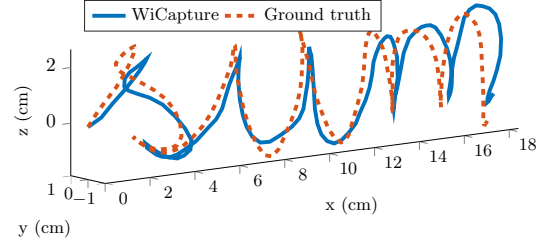


Figure 1. Solid blue path estimated by WiCapture is compared against the dotted red ground truth trajectory.

RGB and depth sensing) and implement vision based tracking algorithms on the headset. These systems are both accurate and infrastructure-free, however they come with certain limitations. Specifically, they significantly increase the complexity of the headset since they need to have several cameras as well as complex algorithms running on the headset to provide tracking. Further they are not robust, tracking fails in environments with transparent or texture-less objects (e.g. a white wall) [60]. Finally and most importantly, these systems cannot be used for tracking peripherals such as hand-motion controllers; the complexity of inside out tracking is too high to be implemented on such peripherals which are meant to be lightweight and cheap.

In this paper, we present WiCapture, a novel VR position tracking system which addresses the above limitations of existing systems. WiCapture is a WiFi based position tracking system. Headsets transmit standard WiFi packets which are received by standard WiFi access points (APs). The WiFi APs also receive metadata from each WiFi packet reception called Channel State Information (CSI) which encodes the transformation the environment has induced upon the transmitted WiFi signals. WiCapture invents novel algorithms that mine the CSI metadata to recover the position of the headset accurately. It has the following properties:

- WiCapture does not require special hardware, it uses commodity APs that can be bought in any retail store.
- WiCapture is occlusion resistant, it continues to work even when the APs and headsets are occluded due to furniture or other objects in between.

- WiCapture has room level range.
- It is insensitive to room illumination or texture, it can work in the dark. Further, headset complexity is minimal, all the headset needs is a standard WiFi chip.

At a high level, as illustrated in Fig. 2, WiCapture obtains the change in the position of the transmitter by using the change in the phase of the CSI between packets. As with the ToF (Time of Flight) cameras, the phase is distorted due to the signal received from reflectors; this phenomenon is called multipath propagation. However, unlike ToF cameras where the light transmitter and camera are time-synchronized, the phase of WiFi signal is also distorted due to the lack of synchronization of clocks at the WiFi transmitter and receiver. WiCapture tackles these challenges using novel algorithms that compensate for these distortions and provides accurate phase measurement which in turn enables accurate position tracking.

1.1. Contributions

- WiCapture is the *first* commodity WiFi-based sub-centimeter level accurate tracking system.
- WiCapture is the *first* system that accurately resolves multipath by using CSI from multiple packets. The key observation is that direction of the paths remain stationary over small intervals of time and CSI of all the packets obtained within this time can be used to resolve multipath accurately.
- We *developed* a novel technique to overcome the distortion due to clock differences by exploiting the multipath. This is surprising as multipath is traditionally viewed as a complication in wireless localization [33] and ToF camera systems [11].
- We *built* WiCapture using commodity Intel 5300 WiFi chips [26] which demonstrated a precision of 0.25 mm and a position tracking error of 0.88 cm.

1.2. Limitations

WiCapture’s current prototype however has two limitations compared to existing systems. It has higher latency since the tracking is computed in the network and then provided as an update to the headset. Second, it is less accurate than current outside-in position tracking systems. We believe that WiCapture’s accuracy is acceptable for VR given the significant benefits that WiCapture provides around deployment, coverage and occlusion resistance.

2. Related work

Motion tracking has been of great interest with applications in 3D object reconstruction, virtual/augmented reality, motion capture and motion control [55, 38]. Systems requiring infrared LEDs or photodiodes on the tracked object have short-range, limited field of view, difficulty in tracking multiple objects, and require line of sight between tracked ob-

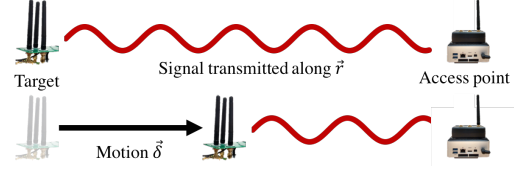


Figure 2. The change in the phase of CSI can be modeled in terms of the displacement of the target and the direction of the transmitted signal. WiFi waves in 5GHz spectrum have 6 cm wavelength. So, even millimeter-level motion creates measurable phase shift.

ject and sensor [34, 3, 60, 28, 46]. Pulsed laser light based systems, in addition, require time synchronization of multiple laser light sources [28]. WiCapture does not share these limitations as it has long range and typical obstructions like walls and humans are transparent to WiFi signals.

Magnetic signal-based systems [45, 4] are occlusion-resistant but have a small range and are affected by distortions due to ferromagnetic materials [53]. Radio frequency signal based techniques using RFIDs (Radio Frequency IDentification) [52, 59] and ultrawideband [23] signals demonstrated centimeter-level accuracy but have limited range and require specialized infrastructure that is not as ubiquitous as WiFi. Tracking systems using other modalities like ultrasound [21, 49] and IR [5, 16] achieve high accuracy but require infrastructure dedicated for tracking.

Infrastructure-free approaches using inertial measurement units (IMUs) can only track the orientation of a device but not the position [20]. Visual-inertial navigation systems [19, 42, 14] which use cameras and IMUs track the motion of a camera using natural image features unlike earlier systems [54] which required instrumentation of the environment with markers. However, visual systems have problems in environments with transparent or textureless objects [60] and are not applicable when the camera is occluded; for example, a phone cannot track itself when placed in a user’s pocket. However, when they are applicable, we view WiCapture and infrastructure-free systems as complementary solutions that together can potentially form a robust and easy-to-deploy motion tracking system.

Disentangling multipath is a widely studied problem in Time of Flight (ToF) cameras and wireless literature as it enables several important applications like transient light imaging [43, 36, 39], wireless imaging [8, 9] and localization [33, 51]. [24, 22, 32, 18, 27, 17, 11, 36, 30] explored transmitting signals at multiple frequencies to resolve multipath in ToF cameras. Similarly, wireless localization systems [33, 56] explored using multiple frequencies to resolve multipath. Unlike all the previous systems, we use signal received from multiple packets to improve the accuracy of estimated multipath parameters. This hinges on the fact that multipath parameters like direction of the propagation paths are stationary over small time periods.

WiFi-based localization systems can be broadly classified into signal strength (called RSSI) based, ToF based, and AoA based systems. Signal strength based systems have 2-4 m accuracy [10, 15, 25] because of distortions in RSSI due to multipath. RSSI fingerprint-based approaches [61, 40] achieve 0.6 m localization error but require an expensive, recursive fingerprinting operation. ToF based approaches achieve meter-level localization error [37, 58, 51]. AoA based approaches achieved state-of-the-art decimeter-level localization error [33, 57, 35, 48, 29]. WiCapture on the other hand is targeted towards estimating trajectory rather than the absolute position. WiFi-based tracking systems [62] can only classify the trajectory of the target WiFi device into limited number (four) of known gestures.

Techniques-wise, [50] theoretically observed that stationarity of multipath parameters improves multipath estimation accuracy. [44] removed the effect of time offset between laser source and camera receiver on the ToF measurements by considering differential ToF between different rays. WiCapture builds on these techniques and compensates not only for time offset but also frequency offset between the source and the receiver.

3. Preliminaries

In WiFi communication systems, the transmitter sends sinusoidal signals of multiple frequencies; each frequency is called a subcarrier [7]. In today's chips, the signal is also typically transmitted on multiple antennas to increase the data rate. For every WiFi packet received, any commercial WiFi chip calculates Channel State Information (CSI) which is the amplitude and phase of the signal received from all the transmitter antennas at all the frequencies. WiCapture reuses this CSI to accurately track the trajectory of the transmitter. We provide a brief primer on CSI modeling.

3.1. CSI calculation

Consider a particular complex sinusoid signal $e^{j2\pi f_n t}$ corresponding to n^{th} subcarrier of frequency f_n emitted by the q^{th} antenna on the transmitter; here j is the complex root of -1 and t is time. This signal passes through the wireless channel, $h_{q,n}$, gets demodulated (see Eq. 1) by the local sinusoid at the receiver, and result is the CSI for that particular antenna-subcarrier pair, $\hat{h}_{q,n}$. Mathematically,

$$\hat{h}_{q,n} = \frac{1}{T} \int_0^T h_{q,n} e^{j2\pi f_n t} e^{-j2\pi f_n t + j\nu} dt = h_{q,n} e^{j\nu}, \quad (1)$$

where T is time for which sinusoid is transmitted and ν is the phase of the receiver's local sinusoidal signal relative to the phase of the transmitter's sinusoidal signal (see Fig. 4).

In indoor environments, transmitted signal travels along multiple paths and the signals from all the paths superpose to form the received signal. Each path is associated with an AoD (Angle of Departure) from the transmitter and atten-

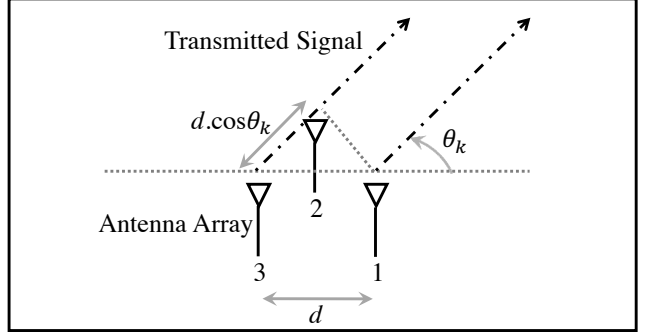


Figure 3. Uniform circular array consisting of 3 antennas: For AoD of θ_k , the target's signal travels an additional distance of $d * \cos(\theta_k)$ from the third antenna in the array compared to the signal from the first antenna. This results in an additional phase of $-2\pi * d * \cos(\theta_k) / \lambda$ for the signal received from the third antenna compared to that from the first antenna.

uation of the signal along the path. We now describe the relation between the wireless channel $h_{q,n}$ and these path parameters. For this description, we consider the circular 3-antenna array used by WiCapture although the model can be extended to any arbitrary antenna array geometry.

3.2. Wireless channel modeling

Consider an environment with L paths; *e.g.*, setup in Fig. 5(b) has 2 paths. Let the spacing between any two antennas in the 3-antenna circular array at the transmitter be d . Let the AP/receiver be in the same plane as the transmitter antenna array. Let θ_k denote the angle of departure (AoD) from the transmitter for the k^{th} path using the convention shown in Fig. 3. Let $\gamma_{k,n}$ denote the signal received along k^{th} path from the first transmitter antenna on the n^{th} subcarrier to the receiver antenna.

The signal along k^{th} path travels different distances from different transmit antennas to the receiver and hence, the signal from different antennas accumulate different phases. So, as described in [57] and illustrated in Fig. 3, the vector of signals received from the transmit antennas along k^{th} path can be written as $\vec{a}(\theta_k) \gamma_{k,n}$, where

$$\vec{a}(\theta_k) = [1 \ e^{-j2\pi * d * \cos(\theta_k + \pi/3) / \lambda} \ e^{-j2\pi * d * \cos(\theta_k) / \lambda}]^T. \quad (2)$$

This vector $\vec{a}(\theta_k)$ is also known as the steering vector. We have as many steering vectors as the number of paths.

The overall attenuation and phase shift introduced by the environment, which is the wireless channel $h_{q,n}$, is obtained by summing the signals received from all the paths. So,

$$\mathbf{H} = [\vec{a}(\theta_1) \ \dots \ \vec{a}(\theta_L)] \mathbf{F} = \mathbf{A} \mathbf{F}, \quad (3)$$

where N is the number of subcarriers, $\mathbf{H} \in \mathbb{C}^{3 \times N}$ is the wireless channel matrix whose element in q^{th} row and n^{th} column is $h_{q,n}$, $\mathbf{F} \in \mathbb{C}^{L \times N}$ is the matrix of complex attenuations whose element in k^{th} row and n^{th} column is $\gamma_{k,n}$,

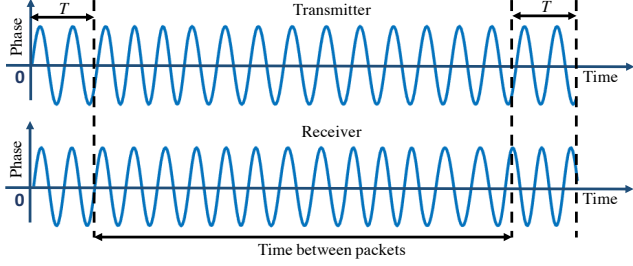


Figure 4. T in Eq. 1 is on the order of few microseconds which is very small compared to the time interval between successive WiFi transmissions which is on the order of milliseconds. So, the relative phase can be assumed to be constant for T period but changes on the order of few hundred radians within few milliseconds.

$\mathbf{A} \in \mathbb{C}^{3 \times L}$ is the steering matrix whose k^{th} column is the steering vector for k^{th} path.

Let $\hat{\mathbf{H}} \in \mathbb{C}^{3 \times N}$ be the observed CSI matrix whose element in q^{th} row and n^{th} column is $\hat{h}_{q,n}$. $\hat{\mathbf{H}}$ would be related to the observed CSI matrix using the relation, $\hat{\mathbf{H}} = \mathbf{H} * e^{j\nu}$.

3.3. Change in channel due to displacement

We will now describe how the transmitter's motion affects the wireless channel. For the rest of the paper, we will index the CSI with corresponding packet, i.e., $\hat{\mathbf{H}}_p \in \mathbb{C}^{3 \times N}$ is CSI for p^{th} packet and $\mathbf{H}_p \in \mathbb{C}^{3 \times N}$ represents the corresponding wireless channel. Let's say the transmitter moved by a small displacement $\vec{\delta}$ between two consecutive packets. Then the path-length for the k^{th} path changes by $\vec{r}_{\theta_k}^T \cdot \vec{\delta}$ where \vec{r}_{θ_k} is the unit vector along the direction of departure for the particular path with AoD θ_k . This induces a phase shift, $2 * \pi * (\vec{r}_{\theta_k}^T \cdot \vec{\delta}) / \lambda$. Mathematically, if $\mathbf{H}_1 = \mathbf{A}\mathbf{F}$ as in Eq. 3, then the wireless channel for the second packet is

$$\mathbf{H}_2 = \mathbf{A}\mathbf{D}\mathbf{F}, \quad (4)$$

where $\mathbf{H}_2 \in \mathbb{C}^{3 \times N}$, $\mathbf{A} \in \mathbb{C}^{3 \times L}$, $\mathbf{F} \in \mathbb{C}^{L \times N}$, and $\mathbf{D} \in \mathbb{C}^{L \times L}$ is a diagonal matrix with entries $e^{-j2\pi * (\vec{r}_{\theta_1}^T \cdot \vec{\delta}) / \lambda}$, ..., $e^{-j2\pi * (\vec{r}_{\theta_{L-1}}^T \cdot \vec{\delta}) / \lambda}$, and $e^{-j2\pi * (\vec{r}_{\theta_L}^T \cdot \vec{\delta}) / \lambda}$.

3.4. Phase distortion due to frequency offset

The transmitter and the receiver WiFi chips have different clocks and this creates an offset between the frequencies of the local sinusoids used at the transmitter and the receiver. Moreover, the offset is not constant with time as the clocks drift [63, 13]. As illustrated in Fig. 4, the frequency offset results in a change in the relative phase between the sinusoids at the transmitter and the receiver (see Equation 1) from packet to packet. Let ν_p be the relative phase between the two sinusoids for p^{th} packet. Then,

$$\hat{\mathbf{H}}_p = \mathbf{H}_p e^{j\nu_p}. \quad (5)$$

So, if the transmitter moved by $\vec{\delta}$ between consecutive packets, then using Equations 3, 4 and 5, the CSI reported by

the WiFi chip for the two packets can be written as

$$\hat{\mathbf{H}}_1 = \mathbf{A}\mathbf{F}e^{j\nu_1}, \hat{\mathbf{H}}_2 = \mathbf{A}\mathbf{D}\mathbf{F}e^{j\nu_2}. \quad (6)$$

Eq. 6 relates the observed CSI to the transmitter's displacement. It is important to note that frequency offset of 20 kHz is typical and WiFi standard allows it to be as high as 200 kHz [7]. This implies that the distortion in CSI due to frequency offset is orders of magnitude greater than the change caused by transmitter's motion. For example, if two consecutive WiFi packets are sent with a time-gap of 10 ms (which is typical), then the relative phase between the transmitter and receiver sinusoids can change by 630 radians and is observed in practice [41]. To compare, if the transmitter moved by 5 mm during the same 10 ms, then the change in the phase of any path is less than 0.6 radians.

4. Design

Fig. 5(a) shows how WiCapture would be deployed. The target transmits normal WiFi packets. A central server collects CSI measurements from all the access points for each packet. The server uses CSI to determine the position of the target by performing the following two steps:

1. Estimate AoD and complex attenuation of all the paths.
2. Use the attenuation from consecutive packets along with AoD of the paths to estimate the displacement of the transmitter between the packets.

4.1. Estimating AoD of all the paths

Let's rewrite the CSI for the first packet from Eq. 6 as $\hat{\mathbf{H}}_1 = \mathbf{A}(\mathbf{F}e^{j\nu_1})$. This is standard form for applying well-known MUSIC algorithm to compute AoD [47, 33, 56]. The goal of the MUSIC algorithm is to find all the steering vectors given multiple linear combinations of the steering vectors. Here, each column of the steering matrix $\mathbf{A} \in \mathbb{C}^{3 \times L}$ is a steering vector and different columns of CSI matrix $\hat{\mathbf{H}}_1 \in \mathbb{C}^{3 \times N}$ are obtained by different linear combinations of the steering vectors. Once the steering vectors are obtained, finding the AoD of all the paths is trivial using Eq. 2.

We omit the mathematical derivation for brevity, but we can show the following: *the eigenvectors corresponding to zero eigenvalues of $\hat{\mathbf{H}}_1 \hat{\mathbf{H}}_1^*$ are orthogonal to the steering vectors in \mathbf{A}* ¹. So the MUSIC algorithm at a basic level proceeds first by computing $\hat{\mathbf{H}}_1 \hat{\mathbf{H}}_1^*$, then computing the eigenvectors corresponding to its zero eigenvalues, and then finding the steering vectors orthogonal to these vectors.

The key problem however is the assumption that there are zero eigenvalues of the matrix $\hat{\mathbf{H}}_1 \hat{\mathbf{H}}_1^*$. There is always noise in physical measurements and none of the eigenvalues are really zero. Prior work [50] has theoretically investigated that the more number of linear combinations of steering vectors with independent weights are provided, the

¹ \mathbf{B}^* is conjugate transpose of \mathbf{B} .

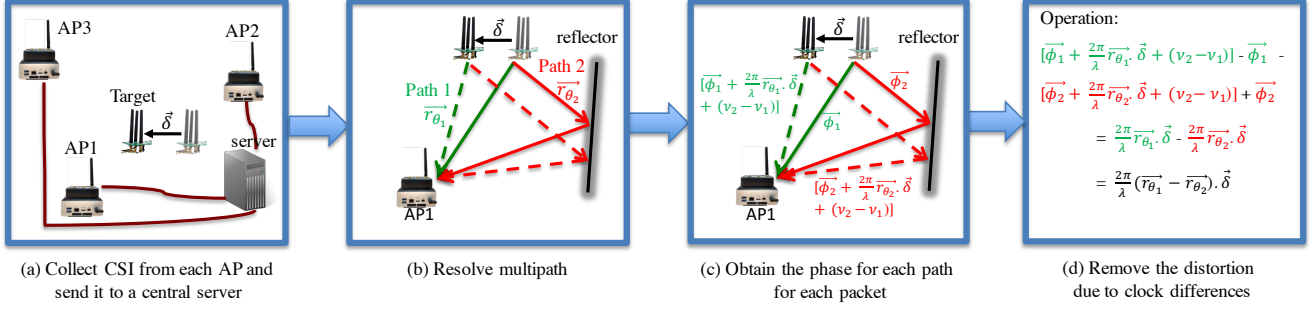


Figure 5. Target moves by $\vec{\delta}$. The new position of the target is shown with solid target icon and the old position with shaded icon. In the first step, for each AP, WiCapture obtains unit vectors along the direction of departure of all the paths. Here, there are two paths, green and red paths, with directions \vec{r}_{θ_1} and \vec{r}_{θ_2} . The paths for first packet are shown using solid lines and the paths for the second packet using dashed lines. Next, the phase of complex attenuation along both the paths for both the packets is calculated. Finally, the effect of frequency offset on the phase values is removed to obtain equations dependent on just \vec{r}_{θ_1} , \vec{r}_{θ_2} and $\vec{\delta}$, which can be solved to estimate $\vec{\delta}$.

higher the accuracy of the estimated steering matrix as the condition number (the ratio of the largest and the smallest singular values) of the matrix $\hat{\mathbf{H}}_1 \hat{\mathbf{H}}_1^*$ increases.

We observe that AoDs of paths are relatively stationary and do not change rapidly from packet to packet. For example, if the receiver is 3 m away from the transmitter, a tiny motion of 1 mm changes the AoD of any path by at most 0.02 degrees, which does not cause any measurable changes in the elements of the steering matrix.

Using this insight, CSI from P packets where AoD hasn't changed much are concatenated using Eq. 7. CSI for any of these packets is linear combination of the same steering vectors. So,

$$\mathbf{X} = [\hat{\mathbf{H}}_1 \hat{\mathbf{H}}_2 \dots \hat{\mathbf{H}}_P] = \mathbf{A}\mathbf{G}, \quad (7)$$

where $\mathbf{X} \in \mathbb{C}^{3 \times PN}$, $\mathbf{A} \in \mathbb{C}^{3 \times L}$ is steering matrix which is common for all the P packets, $\mathbf{G} \in \mathbb{C}^{L \times PN}$ is a matrix of steering vector weights. This is again in standard form for MUSIC and one can apply MUSIC algorithm on \mathbf{X} instead of $\hat{\mathbf{H}}_1$. Since we now provide more number of diverse linear combinations of steering vectors, MUSIC algorithm provides more accurate estimates of AoDs of all the paths.

4.2. Estimating the displacement of the transmitter between consecutive packets

We will now show how the displacement of the WiFi transmitter between two consecutive packets can be estimated. Consider the CSI from the first two packets.

Estimate the weights in linear combination of steering vectors: Each column in the observed CSI matrix is a linear combination of steering vectors estimated using procedure in Sec. 4.1. For p^{th} packet, we now estimate the weights in this linear combination, $\hat{\mathbf{F}}_p \in \mathbb{C}^{L \times N}$, using

$$\hat{\mathbf{F}}_p = \mathbf{A}^\dagger \hat{\mathbf{H}}_p. \quad (8)$$

² \mathbf{B}^\dagger is the pseudo-inverse of \mathbf{B} .

Substituting Eq. 6 into Eq. 8, we can observe that

$$\hat{\mathbf{F}}_1 = \mathbf{F}e^{j\nu_1}, \hat{\mathbf{F}}_2 = \mathbf{D}\mathbf{F}e^{j\nu_2} \quad (9)$$

Estimate the change in the phase of signal for each of the paths: Note that $\mathbf{D} \in \mathbb{C}^{L \times L}$ and its entries contain information about target's displacement (see Eq. 4). We obtain an estimate \mathbf{D} by solving the convex optimization problem 10 using standard procedures [12].

$$\begin{aligned} & \underset{\mathbf{D}}{\text{minimize}} \quad \|\hat{\mathbf{F}}_2 - \mathbf{D}\hat{\mathbf{F}}_1\| \\ & \text{subject to} \quad \mathbf{D} \text{ is diagonal.} \end{aligned} \quad (10)$$

From Equations 9, 10 and 4, the k^{th} diagonal element of \mathbf{D} , $\mathbf{D}_{k,k}$, is an estimate of $e^{-j2\pi * (\vec{r}_{\theta_k}^\top \cdot \vec{\delta}) / \lambda + j\nu_2 - j\nu_1}$. One can obtain unit vector in the direction of the departure using $\vec{r}_{\theta_k} = [\cos(\theta_k) \sin(\theta_k)]^\top$; here θ_k is the AoD for the particular path estimated using procedure in Sec. 4.1.

So, if the term $(\nu_2 - \nu_1)$ is removed, one can estimate $\vec{\delta}$ from the phase of elements of \mathbf{D} . However, as discussed in Sec. 3.4, the term $\nu_2 - \nu_1$ due to frequency offset is orders of magnitude larger than the term $-2\pi * (\vec{r}_{\theta_k}^\top \cdot \vec{\delta}) / \lambda$ due to displacement. This change in phase due to frequency offset is not only unavailable but also extremely hard to predict [13] making it hard to estimate and remove the term $\nu_2 - \nu_1$. This is precisely the phenomenon that led to long-held notions like phase information across packets is unusable for tracking and is uncorrelated in commodity WiFi systems [41].

Use relative phase-change between paths: Our unique insight is that one can get rid of the effect of frequency offset by using the phase of the signal from multiple paths. This is surprising as multipath is traditionally viewed as a complication/challenge in wireless localization and ToF camera systems [33, 31]. Notice that the effect of frequency offset is the same for all the paths, *i.e.*, the term, $\nu_2 - \nu_1$, is present in the change of phase for all the paths. So, effect of the clock differences is removed by considering the change in the phase of signal along a path with respect to change in

the phase of signal from another path.

Specifically, consider the phase of the complex number $\mathbf{D}_{k+1,k+1}/\mathbf{D}_{1,1}$. It is an estimate of $(-2\pi * \vec{r}_{\theta_{k+1}}^\top \cdot \vec{\delta}/\lambda + \nu_2 - \nu_1) - (-2\pi * \vec{r}_{\theta_1}^\top \cdot \vec{\delta}/\lambda + \nu_2 - \nu_1) = (-2\pi * (\vec{r}_{\theta_{k+1}} - \vec{r}_{\theta_1})^\top \cdot \vec{\delta}/\lambda)$. Notice that the term, $\nu_2 - \nu_1$, canceled out by performing this operation. So, a $(L-1)$ -dimensional vector \vec{s} is calculated whose k^{th} element is

$$\vec{s}_k = \text{phase of } (\mathbf{D}_{k+1,k+1}/\mathbf{D}_{1,1}). \quad (11)$$

Then $\mathbf{R} \in \mathbb{R}^{(L-1) \times 2}$ is calculated whose k^{th} row is

$$\frac{-2\pi}{\lambda} * [(\cos(\theta_{k+1}) - \cos(\theta_1)) \quad (\sin(\theta_{k+1}) - \sin(\theta_1))]. \quad (12)$$

One can then obtain an estimate of the displacement by solving the simple linear least squares problem 13.

$$\vec{\delta} = \text{argmin } \|\mathbf{R}\vec{\delta} - \vec{s}\|. \quad (13)$$

If there are multiple APs, matrix \mathbf{R} and vector \vec{s} obtained from multiple access points are concatenated vertically. If there are L paths from the target to each of the U APs, then the concatenated $\mathbf{R} \in \mathbb{R}^{U*(L-1) \times 2}$ and the concatenated $\vec{s} \in \mathbb{R}^{U*(L-1)}$. Since the target displacement is same irrespective of the AP, one can estimate of the displacement by solving Eq. 13 using these concatenated matrices. We summarize the overall algorithm in Algorithm 1.

Algorithm 1: WiCapture's motion tracking algorithm

Data: CSI of packets from target to each of the U APs

Result: Trajectory traced by the target

- 1 Initiate the trajectory at origin ;
 - 2 **for** each packet p received at APs **do**
 - 3 Consider packets received within the last V seconds. Let the number of such packets be P ;
 - 4 Form \mathbf{X} from CSI of P packets using Eq. 7 ;
 - 5 Apply MUSIC [47] on \mathbf{X} to find AoD of L paths ;
 - 6 Obtain the steering vector weights using Eq. 8 ;
 - 7 Obtain change in complex attenuation between p^{th} and $(p+1)^{\text{th}}$ packets by solving 10 ;
 - 8 Form \mathbf{R} using Eq. 12 and \vec{s} using Eq. 11 ;
 - 9 Update the trajectory by adding displacement obtained by solving 13 ;
 - 10 **end**
-

5. Implementation

We implemented WiCapture using off-the-shelf Intel 5300 WiFi cards which support three antennas. We employed Linux CSI tool [26] to obtain the CSI for each packet. The WiFi cards operate in 5 GHz WiFi spectrum using 40 MHz bandwidth. Also, the CSI information is quantized, i.e., each of real and imaginary parts of CSI for every subcarrier is represented using 8 bits.

The system used for evaluation consists of APs and a target device equipped with WiFi cards. The target has three

antennas with distance between any two antennas equal to 2.6 cm. Each AP has three antennas in a uniform linear array with distance between successive antennas equal to 2.6 cm. In Sec. 4.1, we described AoD estimation when the AP/receiver has only one antenna. CSI obtained from multiple receive antennas is used to improve the accuracy of AoD estimates. The APs operate in monitor mode. The target transmits a packet every 6 ms. So, the trajectory is estimated at an update rate of 167 Hz for our evaluation experiments. We implemented the Algorithm 1 in MATLAB. We use $U = 4$ APs, set $V = 10$ s and $L = 2$ paths in Algorithm 1. We will make the source code and data available.

6. Evaluation

6.1. Stationary experiments

We start by examining the jitter/precision of WiCapture, i.e., how stationary the estimated position is when the target is stationary. This is important for VR because the scene displayed on the VR headset is not expected to change when the user is not moving. In our experiment, the target remains stationary and transmits 1000 packets. The access points are placed at the corners of $5 \text{ m} \times 6 \text{ m}$ space. The standard deviation of the trajectory obtained by using Algorithm 1 is used as the measure of jitter. The median jitter observed over 21 experiments at different target positions is 0.25 mm.

We measured the jitter of Oculus DK2 system by placing it at the same positions. The Oculus camera is placed at 0.75 m away from the headset. The median jitter observed for Oculus DK2 is 0.10 mm. So, WiCapture's jitter in position estimation is comparable to that of a commercial position tracking system which requires dedicated infrastructure.

6.2. Controlled tracking experiments

Next we evaluate the resolution of WiCapture. We mount the target on a mechanical stage which has a least count error of 0.005 cm. The target is moved in increments of 0.1 cm and then in decrements of 0.1 cm so that it reaches the initial position as shown in Fig. 6(a). The target transmits a WiFi packet at each position. Trajectory estimated by WiCapture is translated so that the initial position is origin. The maximum error in estimation of position of any point in the trajectory is 0.11 cm.

We conducted another experiment where the target is moved mechanically to different positions on a trajectory shown in Fig. 6(b). The maximum error in estimation of position of any point in the trajectory is 0.27 cm. Note that WiCapture resolves even millimeter-level target motion.

6.3. Extensive tracking experiments

Motion tracking accuracy of WiCapture is dependent on the multipath environment, the material used in walls, the

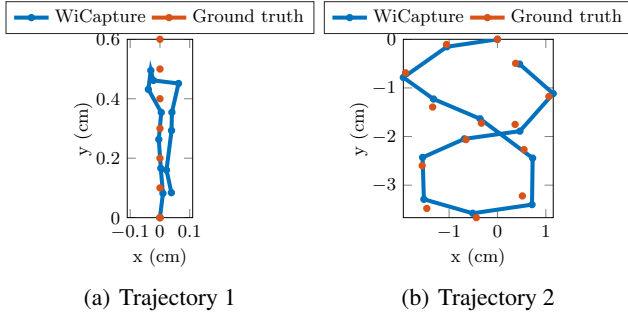


Figure 6. Controlled trajectories where the target is positioned at different locations in a trajectory mechanically.

presence of metallic objects, the density of WiFi AP deployment and many other factors. In this evaluation, we test WiCapture’s accuracy in different deployment scenarios.

Compared Approaches: To the best of our knowledge, there exists no WiFi-based system that is geared towards *tracking* the motion of a commodity WiFi chip. We faithfully implemented SpotFi, a state-of-the-art WiFi localization system and compared WiCapture against it.

Ground truth: We use an Oculus DK2 [6] headset which is rigidly attached to the target to obtain ground truth trajectory. We placed the headset 0.9 m away from the Oculus camera. Under these conditions, we calculated the accuracy of Oculus position tracking to be at sub-millimeter levels using mechanical stage experiments (see Sec. 6.2).

Metric (Trajectory error): To focus on the shape of the trajectory alone, we translate the trajectory reported by each of the systems (Oculus DK2, SpotFi and WiCapture) by the initial position of the trajectory so that the initial position of all the trajectories is origin. Similarly, since the reference coordinate axes of different systems are not aligned, we rotate the trajectory reported by WiCapture (and SpotFi) so that the Root Mean Squared Error (RMSE) between the points of the rotated trajectory of WiCapture (and SpotFi) and the points on the Oculus trajectory is minimized. Note that we just shift and rotate the trajectories of WiCapture and SpotFi but do not scale the trajectories. As in other motion tracking systems [52], absolute point-by-point position difference between this shifted and rotated trajectories and the ground truth trajectory is reported as the trajectory error.

6.3.1 Indoor office deployment

Method: We start by deploying WiCapture in a $5\text{ m} \times 6\text{ m}$ room with access points deployed at the four corners and the target is placed in the same room. This is the typical access point deployment density used in state-of-the-art WiFi localization systems like SpotFi [33]. We traced 97 trajectories with the target device. The target was moved in a continuous manner on a table rather than point by point as done in Sec. 6.2. Fig. 7(a) shows the experimental setup. A sample trajectory is shown in Fig. 1.

Analysis: From Fig. 8(a), WiCapture achieves a median trajectory error of 0.88 cm. SpotFi’s median trajectory error, 132 cm, is more than two orders of magnitude larger than that of WiCapture. WiCapture thus achieves centimeter-level motion tracking using commodity WiFi cards.

6.3.2 Occlusion deployment

Method: We evaluate WiCapture under challenging conditions where the target is one room and all the APs are occluded from the target either by furniture or by walls. Fig. 7(b) shows the experimental setup which shows couple of APs where one AP is placed outside the room where the target is placed and another AP is separated from the target through a cubicle. We traced 64 different trajectories.

Analysis: Fig. 8(b) plots the CDF of the trajectory error of WiCapture and SpotFi when either one or two access points are outside the room where the target is placed. However, note that all the access points are occluded whether they are inside the target’s room or not. Under these conditions, WiCapture achieves a median trajectory error of 1.51 cm. Thus, even in the challenging conditions where the target is occluded from the positioning system, WiCapture achieves accuracy acceptable for many applications.

We further stress-tested by placing three or more APs outside the room at which point the reconstructed trajectories accumulated large errors. So, WiCapture can provide accurate tracking only when atleast two access points are present which are not separated from the target by walls.

6.3.3 Outdoor deployment

Method: We evaluate WiCapture in a $5\text{ m} \times 6\text{ m}$ outdoor space. The experiments are conducted in shade for accurate Oculus measurements. Fig. 7(c) shows the experimental setup. We traced 89 trajectories.

Analysis: From Fig. 8(c), WiCapture achieves a median trajectory error of 0.85 cm compared to SpotFi’s 57 cm trajectory error. Thus, WiCapture can ubiquitously track a commodity WiFi device as long as there is WiFi infrastructure irrespective of whether the target is indoors or outdoors.

6.4. Deep dive into WiCapture

WiCapture achieves accurate motion tracking due to two novel techniques. First, WiCapture accurately resolves multipath by using multiple packets for estimation. Second, WiCapture accurately removes the phase distortion due to frequency offset between the transmitter and the receiver. We now test the significance of each of these factors individually. For the following experiments, we consider the data from the indoor office deployment scenario in Sec. 6.3.1.

6.4.1 Improved AoD estimation

Method: We compare WiCapture against an alternate method which uses single packet for AoD estimation (set P equal to 1 in Eq. 7). AoD estimation error of a particular method (single packet or multiple packets) is measured

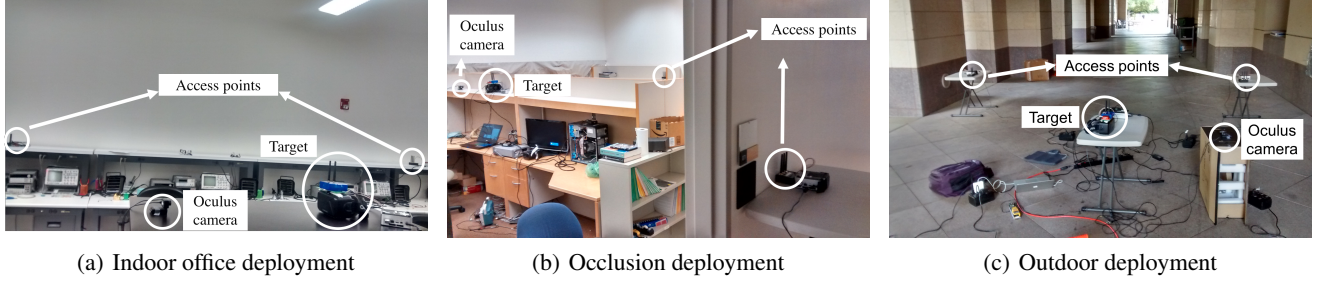


Figure 7. Experiment setups for the three deployments

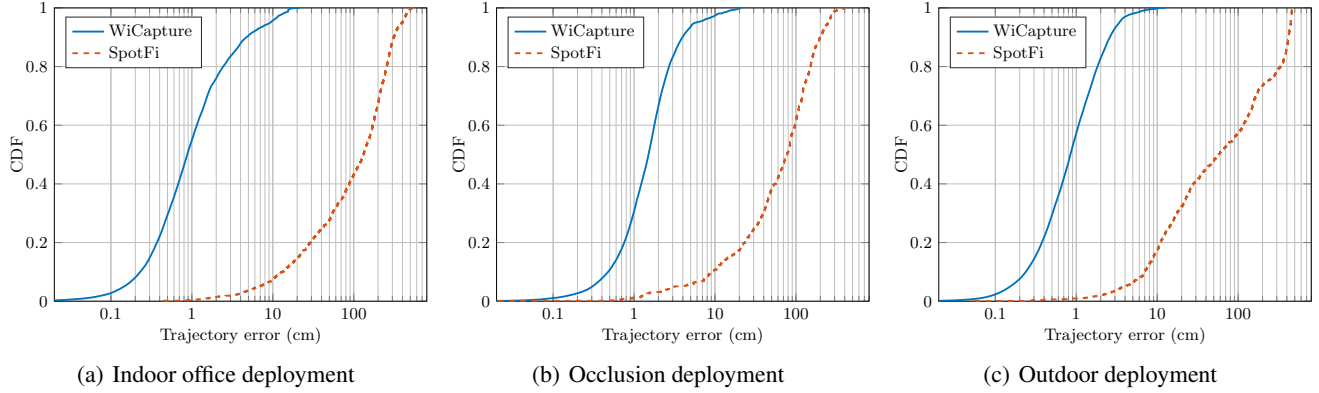


Figure 8. Cumulative Distribution Function (CDF) of trajectory error for the three deployments

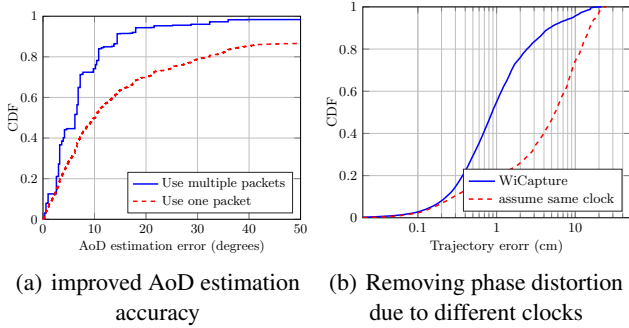


Figure 9. (a) plots the CDF of AoD estimation error when using multiple packets (WiCapture) and when using one packet. (b) plots the CDF of trajectory error when using WiCapture and when using *assume same clock* method which ignores frequency offset.

by using the absolute difference between ground truth direct path AoD (which is measured manually) and AoD estimated using the particular method that is closest to this ground truth.

Analysis: From Fig. 9(a), 80th percentile AoD estimation error by using multiple packets is 11 degrees and is 3 \times smaller than the error obtained by using a single packet.

6.4.2 Removing phase distortion from frequency offset

Method: We compare WiCapture against an alternate method which solves a system of equations where each

equation equates the change in the phase of complex attenuation of a path directly as a linear function of displacement without considering the offset from the clock differences. We call this alternate method as *assume same clock*.

Analysis: From Fig. 9(b), the trajectory estimation errors are 6 \times worse when frequency offset is ignored.

7. Discussion and conclusion

All the major WiFi chip families (Atheros, Intel, and Marvell) expose CSI [26, 48]. Hence, we believe WiCapture can be added to any commodity WiFi infrastructure.

Circular antenna arrays have less accuracy in estimating the direction of the paths in a three-dimensional space restricting the trajectories to be approximately 2D. We plan to use different antenna architectures to enable 3D tracking.

In WiCapture, there is network latency to deliver the position estimates to headset. We plan to use IMU sensors to enable real-time position tracking using WiCapture to correct IMU drifts.

In conclusion, we developed and implemented a WiFi-based motion tracking system and demonstrated its performance in different deployment scenarios. A commodity WiFi-based position tracking system would potentially enable VR on mobile devices and revolutionize number of applications that can be enabled on top of motion tracking.

References

- [1] Htc vive. <https://www.vive.com/>. Accessed: November 2016. 1
- [2] Microsoft hololens. <https://www.microsoft.com/microsoft-hololens/>. Accessed: November 2016. 1
- [3] Oculus rift. <https://www.oculus.com/>. Accessed: November 2016. 1, 2
- [4] Polhemus. <http://polhemus.com/>. Accessed: November 2016. 2
- [5] Vicon. <https://www.vicon.com/>. Accessed: November 2016. 2
- [6] Why virtual reality isnt (just) the next big platform, michael abrash and dov katz of oculus vr. <https://www.youtube.com/watch?v=dxbh-TM5yNc>. Accessed: November 2016. 1, 7
- [7] Ieee standard for information technology– local and metropolitan area networks– specific requirements– part 11: Wireless lan medium access control (mac)and physical layer (phy) specifications amendment 5: Enhancements for higher throughput. *IEEE Std 802.11n-2009 (Amendment to IEEE Std 802.11-2007 as amended by IEEE Std 802.11k-2008, IEEE Std 802.11r-2008, IEEE Std 802.11y-2008, and IEEE Std 802.11w-2009)*, pages 1–565, Oct 2009. 3, 4
- [8] F. Adib, C.-Y. Hsu, H. Mao, D. Katabi, and F. Durand. Capturing the human figure through a wall. *ACM Transactions on Graphics (TOG)*, 34(6):219, 2015. 2
- [9] F. Adib, Z. Kabelac, D. Katabi, and R. C. Miller. 3d tracking via body radio reflections. In *11th USENIX Symposium on Networked Systems Design and Implementation (NSDI 14)*, pages 317–329, 2014. 2
- [10] P. Bahl and V. N. Padmanabhan. Radar: An in-building rf-based user location and tracking system. In *INFOCOM 2000. Nineteenth Annual Joint Conference of the IEEE Computer and Communications Societies. Proceedings. IEEE*, volume 2, pages 775–784. Ieee, 2000. 3
- [11] A. Bhandari, A. Kadambi, R. Whyte, C. Barsi, M. Feigin, A. Dorrington, and R. Raskar. Resolving multipath interference in time-of-flight imaging via modulation frequency diversity and sparse regularization. *Optics letters*, 39(6):1705–1708, 2014. 2
- [12] S. Boyd and L. Vandenberghe. *Convex Optimization*. Cambridge University Press, New York, NY, USA, 2004. 5
- [13] D. R. Brown, R. Mudumbai, and S. Dasgupta. Fundamental limits on phase and frequency tracking and estimation in drifting oscillators. In *2012 IEEE International Conference on Acoustics, Speech and Signal Processing (ICASSP)*, pages 5225–5228. IEEE, 2012. 4, 5
- [14] C. Cadena, L. Carlone, H. Carrillo, Y. Latif, D. Scaramuzza, J. Neira, I. D. Reid, and J. J. Leonard. Past, present, and future of simultaneous localization and mapping: Towards the robust-perception age. *arXiv preprint arXiv:1606.05830*, 2016. 2
- [15] K. Chintalapudi, A. Padmanabha Iyer, and V. N. Padmanabhan. Indoor localization without the pain. In *Proceedings of the sixteenth annual international conference on Mobile computing and networking*, pages 173–184. ACM, 2010. 3
- [16] K. Dorfmueller. Robust tracking for augmented reality using retroreflective markers. *Computers & Graphics*, 23(6):795–800, 1999. 2
- [17] A. A. Dorrington, J. P. Godbaz, M. J. Cree, A. D. Payne, and L. V. Streeter. Separating true range measurements from multi-path and scattering interference in commercial range cameras. In *IS&T/SPIE Electronic Imaging*, pages 786404–786404. International Society for Optics and Photonics, 2011. 2
- [18] D. Droschel, D. Holz, and S. Behnke. Multi-frequency phase unwrapping for time-of-flight cameras. In *Intelligent Robots and Systems (IROS), 2010 IEEE/RSJ International Conference on*, pages 1463–1469. IEEE, 2010. 2
- [19] J. Engel, V. Koltun, and D. Cremers. Direct sparse odometry. *arXiv preprint arXiv:1607.02565*, 2016. 2
- [20] P. Esser, H. Dawes, J. Collett, and K. Howells. Imu: inertial sensing of vertical com movement. *Journal of biomechanics*, 42(10):1578–1581, 2009. 2
- [21] E. Foxlin, M. Harrington, and G. Pfeifer. Constellation: a wide-range wireless motion-tracking system for augmented reality and virtual set applications. In *Proceedings of the 25th annual conference on Computer graphics and interactive techniques*, pages 371–378. ACM, 1998. 2
- [22] D. Freedman, Y. Smolin, E. Krupka, I. Leichter, and M. Schmidt. Sra: Fast removal of general multipath for tof sensors. In *European Conference on Computer Vision*, pages 234–249. Springer, 2014. 2
- [23] S. Gezici, Z. Tian, G. B. Giannakis, H. Kobayashi, A. F. Molisch, H. V. Poor, and Z. Sahinoglu. Localization via ultra-wideband radios: a look at positioning aspects for future sensor networks. *Signal Processing Magazine, IEEE*, 22(4):70–84, 2005. 2
- [24] J. P. Godbaz, M. J. Cree, and A. A. Dorrington. Understanding and ameliorating non-linear phase and amplitude responses in amcw lidar. *Remote Sensing*, 4(1):21, 2012. 2
- [25] A. Goswami, L. E. Ortiz, and S. R. Das. Wigem: A learning-based approach for indoor localization. In *Proceedings of the Seventh Conference on Emerging Networking EXperiments and Technologies, CoNEXT '11*, pages 3:1–3:12, New York, NY, USA, 2011. ACM. 3
- [26] D. Halperin, W. Hu, A. Sheth, and D. Wetherall. Tool release: Gathering 802.11n traces with channel state information. *ACM SIGCOMM CCR*, 41(1):53, Jan. 2011. 2, 6, 8
- [27] F. Heide, M. B. Hullin, J. Gregson, and W. Heidrich. Low-budget transient imaging using photonic mixer devices. *ACM Transactions on Graphics (ToG)*, 32(4):45, 2013. 2
- [28] S. Islam, B. Ionescu, C. Gadea, and D. Ionescu. Full-body tracking using a sensor array system and laser-based sweeps. In *2016 IEEE Symposium on 3D User Interfaces (3DUI)*, pages 71–80, March 2016. 2
- [29] K. Joshi, S. Hong, and S. Katti. Pinpoint: localizing interfering radios. In *Proceedings of the 10th USENIX conference on Networked Systems Design and Implementation*, pages 241–254. USENIX Association, 2013. 3
- [30] A. Kadambi, J. Schiel, and R. Raskar. Macroscopic interferometry: Rethinking depth estimation with frequency-domain

- time-of-flight. In *Proceedings of the IEEE Conference on Computer Vision and Pattern Recognition*, pages 893–902, 2016. 2
- [31] A. Kadambi, R. Whyte, A. Bhandari, L. Streeter, C. Barsi, A. Dorrington, and R. Raskar. Coded time of flight cameras: sparse deconvolution to address multipath interference and recover time profiles. *ACM Transactions on Graphics (ToG)*, 32(6):167, 2013. 5
- [32] A. Kirmani, A. Benedetti, and P. A. Chou. Spumic: Simultaneous phase unwrapping and multipath interference cancellation in time-of-flight cameras using spectral methods. In *2013 IEEE International Conference on Multimedia and Expo (ICME)*, pages 1–6. IEEE, 2013. 2
- [33] M. Kotaru, K. Joshi, D. Bharadia, and S. Katti. Spotfi: Decimeter level localization using wifi. In *ACM SIGCOMM Computer Communication Review*, volume 45, pages 269–282. ACM, 2015. 2, 3, 4, 5, 7
- [34] A. Kumar and P. Ben-Tzvi. Spatial object tracking system based on linear optical sensor arrays. *IEEE Sensors Journal*, 16(22):7933–7940, Nov 2016. 2
- [35] S. Kumar, S. Gil, D. Katabi, and D. Rus. Accurate indoor localization with zero start-up cost. In *Proceedings of the 20th annual international conference on Mobile computing and networking*, pages 483–494. ACM, 2014. 3
- [36] J. Lin, Y. Liu, M. B. Hullin, and Q. Dai. Fourier analysis on transient imaging with a multifrequency time-of-flight camera. In *Proceedings of the IEEE Conference on Computer Vision and Pattern Recognition*, pages 3230–3237, 2014. 2
- [37] A. T. Mariakakis, S. Sen, J. Lee, and K.-H. Kim. Sail: single access point-based indoor localization. In *Proceedings of the 12th annual international conference on Mobile systems, applications, and services*, pages 315–328. ACM, 2014. 3
- [38] K. Meyer, H. L. Applewhite, and F. A. Biocca. A survey of position trackers. *Presence: Teleoperators & Virtual Environments*, 1(2):173–200, 1992. 2
- [39] N. Naik, A. Kadambi, C. Rhemann, S. Izadi, R. Raskar, and S. Bing Kang. A light transport model for mitigating multipath interference in time-of-flight sensors. In *Proceedings of the IEEE Conference on Computer Vision and Pattern Recognition*, pages 73–81, 2015. 2
- [40] R. Nandakumar, K. K. Chintalapudi, and V. N. Padmanabhan. Centaur: locating devices in an office environment. In *Proceedings of the 18th annual international conference on Mobile computing and networking*, pages 281–292. ACM, 2012. 3
- [41] R. Nandakumar, B. Kellogg, and S. Gollakota. Wi-fi gesture recognition on existing devices. *arXiv preprint arXiv:1411.5394*, 2014. 4, 5
- [42] E. D. Nerurkar, K. J. Wu, and S. I. Roumeliotis. C-klam: Constrained keyframe-based localization and mapping. In *2014 IEEE International Conference on Robotics and Automation (ICRA)*, pages 3638–3643. IEEE, 2014. 2
- [43] M. O’Toole, F. Heide, L. Xiao, M. B. Hullin, W. Heidrich, and K. N. Kutulakos. Temporal frequency probing for 5d transient analysis of global light transport. *ACM Transactions on Graphics (ToG)*, 33(4):87, 2014. 2
- [44] R. Pandharkar, A. Velten, A. Bardagjy, E. Lawson, M. Bawendi, and R. Raskar. Estimating motion and size of moving non-line-of-sight objects in cluttered environments. In *Computer Vision and Pattern Recognition (CVPR), 2011 IEEE Conference on*, pages 265–272. IEEE, 2011. 3
- [45] F. H. Raab, E. B. Blood, T. O. Steiner, and H. R. Jones. Magnetic position and orientation tracking system. *IEEE Transactions on Aerospace and Electronic systems*, (5):709–718, 1979. 2
- [46] R. Raskar, H. Nii, B. Dedecker, Y. Hashimoto, J. Summet, D. Moore, Y. Zhao, J. Westhues, P. Dietz, J. Barnwell, et al. Prakash: lighting aware motion capture using photosensing markers and multiplexed illuminators. In *ACM Transactions on Graphics (TOG)*, volume 26, page 36. ACM, 2007. 2
- [47] R. O. Schmidt. Multiple emitter location and signal parameter estimation. *Antennas and Propagation, IEEE Transactions on*, 34(3):276–280, 1986. 4, 6
- [48] S. Sen, J. Lee, K.-H. Kim, and P. Congdon. Avoiding multipath to revive inbuilding wifi localization. In *Proceeding of the 11th Annual International Conference on Mobile Systems, Applications, and Services, MobiSys ’13*, pages 249–262, New York, NY, USA, 2013. ACM. 3, 8
- [49] J. Shin, G. An, J.-S. Park, S. J. Baek, and K. Lee. Application of precise indoor position tracking to immersive virtual reality with translational movement support. *Multimedia Tools and Applications*, pages 1–20, 2016. 2
- [50] M. C. Vanderveen, A.-J. Van der Veen, and A. Paulraj. Estimation of multipath parameters in wireless communications. *Signal Processing, IEEE Transactions on*, 46(3):682–690, 1998. 3, 4
- [51] D. Vasisht, S. Kumar, and D. Katabi. Decimeter-level localization with a single wifi access point. In *13th USENIX Symposium on Networked Systems Design and Implementation (NSDI 16)*, pages 165–178, 2016. 2, 3
- [52] J. Wang, D. Vasisht, and D. Katabi. Rfidraw: Virtual touch screen in the air using rf signals. In *Proceedings of the 2014 ACM Conference on SIGCOMM*, SIGCOMM ’14, pages 235–246, New York, NY, USA, 2014. ACM. 2, 7
- [53] J.-f. Wang, R. T. Azuma, G. Bishop, V. Chi, J. Eyles, and H. Fuchs. Tracking a head-mounted display in a room-sized environment with head-mounted cameras. In *Orlando’90, 16-20 April*, pages 47–57. International Society for Optics and Photonics, 1990. 2
- [54] G. Welch, G. Bishop, L. Vicci, S. Brumback, K. Keller, et al. The hiball tracker: High-performance wide-area tracking for virtual and augmented environments. In *Proceedings of the ACM symposium on Virtual reality software and technology*, pages 1–ff. ACM, 1999. 2
- [55] G. Welch and E. Foxlin. Motion tracking survey. 2002. 2
- [56] Y. Xie, J. Xiong, M. Li, and K. Jamieson. xd-track: leveraging multi-dimensional information for passive wi-fi tracking. In *Proceedings of the 3rd Workshop on Hot Topics in Wireless*, pages 39–43. ACM, 2016. 2, 4
- [57] J. Xiong and K. Jamieson. Arraytrack: A fine-grained indoor location system. In *Presented as part of the 10th USENIX Symposium on Networked Systems Design and Implementation (NSDI 13)*, pages 71–84, Lombard, IL, 2013. USENIX. 3
- [58] J. Xiong, K. Sundaresan, and K. Jamieson. Tonetrack: Leveraging frequency-agile radios for time-based indoor

- wireless localization. In *Proceedings of the 21st Annual International Conference on Mobile Computing and Networking*, pages 537–549. ACM, 2015. [3](#)
- [59] L. Yang, Y. Chen, X.-Y. Li, C. Xiao, M. Li, and Y. Liu. Tago-ram: Real-time tracking of mobile rfid tags to high precision using cots devices. In *Proceedings of the 20th annual international conference on Mobile computing and networking*, pages 237–248. ACM, 2014. [2](#)
- [60] A. Yates and J. Selan. Positional tracking systems and methods, May 2016. [1](#), [2](#)
- [61] M. Youssef and A. Agrawala. The horus wlan location determination system. In *Proceedings of the 3rd International Conference on Mobile Systems, Applications, and Services*, MobiSys '05, pages 205–218, New York, NY, USA, 2005. ACM. [3](#)
- [62] Y. Zeng, P. H. Pathak, C. Xu, and P. Mohapatra. Your ap knows how you move: fine-grained device motion recognition through wifi. In *Proceedings of the 1st ACM workshop on Hot topics in wireless*, pages 49–54. ACM, 2014. [3](#)
- [63] C. Zucca and P. Tavella. The clock model and its relationship with the allan and related variances. *IEEE transactions on ultrasonics, ferroelectrics, and frequency control*, 52(2):289–296, 2005. [4](#)